Journal of Medicinal Chemistry

Article

pubs.acs.org/jmc

Discovery of a Novel Small Molecule Inhibitor Targeting the Frataxin/Ubiquitin Interaction via Structure-Based Virtual Screening and Bioassays

Antonio Lavecchia,*[,†] Carmen Di Giovanni,[†] Carmen Cerchia,[†] Annapina Russo,[‡] Giulia Russo,[‡] and Ettore Novellino[†]

[†]Dipartimento di Chimica Farmaceutica e Tossicologica, "Drug Discovery" Laboratory, Università di Napoli "Federico II", Via Domenico Montesano 49, 80131 Napoli, Italy

[‡]Dipartimento di Biochimica e Biotecnologie Mediche, Università di Napoli "Federico II", Via Sergio Pansini 5, 80131 Napoli, Italy

Supporting Information

ABSTRACT: Friedreich's ataxia (FRDA) is an autosomal recessive neuro- and cardiodegenerative disorder for which there are no proven effective treatments. FRDA is caused by decreased expression and/or function of the mitochondrial protein frataxin. Here, we report findings that frataxin is degraded via the ubiquitin−proteasomal pathway and that it is ubiquitinated at residue K^{147} in Calu-6 cells. A theoretical model of the frataxin-K^{147}/Ub complex, constructed by combining bioinformatics interface predictions with information-driven docking, revealed a hitherto unnoticed, potential ubiquitin-binding domain in frataxin. Through structure-based virtual screening and cell-based assays, we discovered a novel small molecule (compound (+)-**11**) able to prevent frataxin ubiquitination and degradation. (+)-**11** was synthesized and tested for specific binding to frataxin by an UF-LC/MS based ligand-binding assay. Follow-up scaffold-based searches resulted in the identification of a lead series with micromolar activity in disrupting the frataxin/Ub interaction. This study also suggests that frataxin could be a potential target for FRDA drug development.

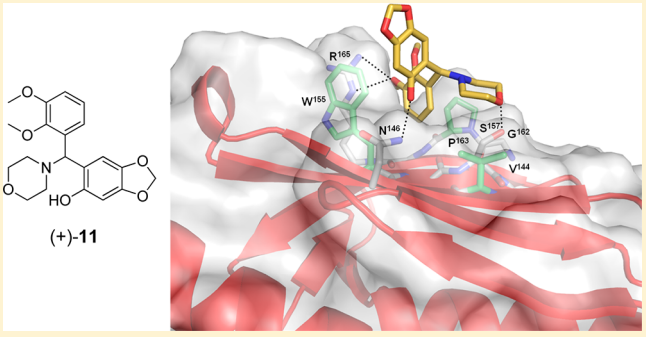

INTRODUCTION

Friedreich's ataxia (FRDA) is an inherited recessive neurodegenerative disorder caused by a partial reduction in levels of the mitochondrial protein frataxin,[1,2] which controls the iron homeostasis. FRDA is the most common inherited form of ataxia with an incidence estimated between 1:30000 to 1:50000 in the U.S. and Europe.[3−5] The disease is characterized by a progressive neuropathy affecting the central and peripheral nervous systems,[6,7] causing death of primary sensory neurons of the dorsal root ganglia and a variable picture of accompanying neurological symptoms.[4] These symptoms tend to appear by the age of 20 in the majority of patients, who are typically normal at birth and during early childhood, although the disease onset is highly variable and can be incomplete and/or delayed for reasons yet to be described.[8] FRDA is caused, in the majority of cases, by an abnormal GAA repeat expansion in the first intron of the human *FRDA* gene,[2] which inhibits transcription,[9] leading in turn to multiple enzyme deficits, mitochondrial dysfunction, and oxidative damage.[10,11] At present there is no effective pharmacological treatment available to slow the progression of the disease.

Frataxin is encoded in the nucleus and synthesized in the cytoplasm as a precursor polypeptide ($frataxin^{1-210}$) that is transported to the mitochondrial matrix and proteolytically cleaved to the mature form ($frataxin^{81-210}$)[12,13] via a processing intermediate ($frataxin^{42-210}$).[14,15] Maturation of the frataxin precursor occurs within the mitochondrial matrix, and no other intramitochondrial post-translational modifications have been identified. Recently, a pool of mature frataxin was detected in the cytoplasm of several cell types of human origin[16−18] where it participates in numerous biological functions.[16,17,19] More recent findings have shown the direct regulation of frataxin precursor and mature accumulation through the ubiquitin−proteasome system (UPS).[20] Thus, small-molecule inhibitors that promote frataxin stabilization are desirable and could potentially have therapeutic value.

Here we report the discovery, synthesis, and characterization of a small molecule (compound (+)-**11**) able to prevent the frataxin ubiquitination and degradation and promote the accumulation of cellular frataxin. To reach this goal, we built a computational model of the frataxin/Ub interaction, using HADDOCK (high-ambiguity-driven docking),[21] a software of wide use in structural biology for protein−protein docking.[22] The putative frataxin Ub-binding domain was chosen for in silico targeting in a multistep structure-based virtual screening

Received: November 21, 2012
Published: March 18, 2013

approach using the National Cancer Institute (NCI) Open Database. The most active compound (±)-**11** was synthesized by a new microwave-assisted procedure, and the resolution of its enantiomers was put forward by a salt crystallization technique. Only the (+)-isomer was active in accumulating both precursor and mature frataxin in human lung adenocarcinoma (Calu-6) cells. The binding affinity of (+)-**11** toward frataxin was proved through an ultrafiltration liquid chromatography/mass spectrometry (UF-LC/MS) based ligand-binding assay.

RESULTS AND DISCUSSION

Frataxin Stability Is Controlled by the UPS in Calu-6 Cells. Previous results showed that proteasomal degradation of both precursor and mature frataxin in human embryonic kidney 293 (HEK-293) cells is mediated by a Ub-dependent mechanism and that K^{147} is the critical residue responsible for frataxin ubiquitination.[20] To validate these findings, we repeated these experiments in Calu-6 cells and analyzed frataxin turnover in the presence and absence of proteasome inhibition. Calu-6 cells, an anaplastic carcinoma of lung origin, were chosen as a model system in this study because they are well characterized, provide a reasonably high transfection efficiency, and express elevated levels of frataxin. Calu-6 cells were transiently transfected with a construct expressing frataxin fused to His tag, and 32 h after transfection cells were treated for 18 h with either 10 μM reversible proteasome inhibitor MG132 (*N*-carbobenzoxyl-L-leucinyl-L-leucinyl-L-leucinal) or 10 μM bortezomib, a peptide boronic acid proteasome inhibitor. Proteins from cell lysates were then analyzed by SDS–PAGE and Western blotting. As shown in Figure 1, the addition of the reversible proteasome inhibitor

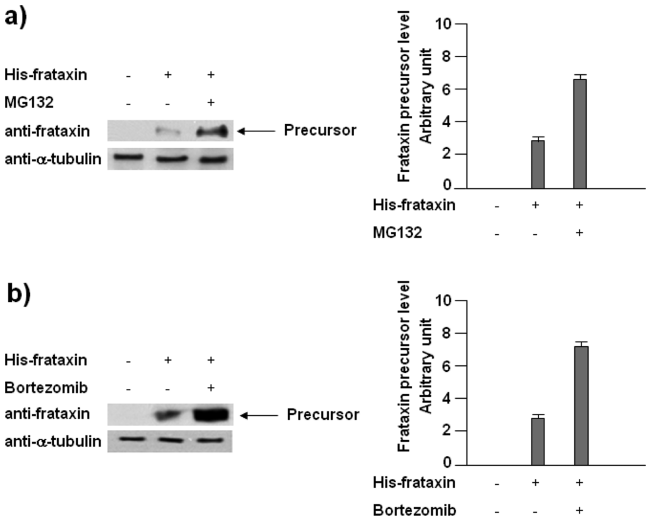

Figure 1. Effect of MG132 and bortezomib on the stability of human frataxin. Western blot analysis with the indicated antibodies of protein extracts from Calu-6 cells untransfected or transfected with His-frataxin and untreated or treated with MG132 (a) or bortezomib (b) for 18 h. The levels of proteins were quantified by PhosphorImager (Bio-Rad, Hercules, CA, U.S.) and normalized to tubulin levels. These results are representative of three independently performed experiments.

MG132 and bortezomib was found to cause a strong increase in frataxin precursor compared to untreated samples.

In order to verify whether the frataxin precursor is targeted to proteasomal degradation by Ub labeling, we went on to perform an immunoprecipitation assay. Calu-6 cells were transiently co-transfected with plasmids expressing both frataxin and Ub fused to His tag (6-histidine) and HA tag (hemagglutinin), respectively. At 24 h after the transfection, cells were treated with 10 μM MG132 for 18 h. Frataxin was then specifically immunoprecipitated from untransfected and transfected cells using anti-frataxin, and the resulting frataxin immunocomplexes were analyzed by SDS–PAGE and Western blotting with antibodies against Ub. As shown in Figure 2, both frataxin and the monoUb-tagged

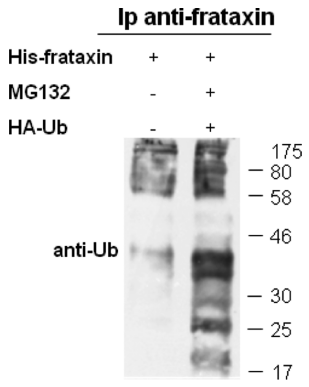

Figure 2. Ubiquitination of frataxin. Frataxin was immunoprecipitated from Calu-6 cells extracts, co-transfected with His-frataxin and HA-Ub, and incubated with 10 μM MG132 for 18 h. Immunoprecipitates were analyzed by Western blotting with anti-Ub antibody. These results are representative of three independently performed experiments.

precursor of frataxin accumulate by MG132 treatment. Interestingly, the detection of a ladder of high molecular weight species characteristic of polyubiquitinated proteins suggested that frataxin is also polyubiquitinated.

To confirm that K^{147} is really the ubiquitination site of frataxin, we altered this residue to R by site-directed mutagenesis and compared the ability of the resulting mutant (His-K^{147}R) to bind to glutathione *S*-transferase (GST) fused Ub (GST-monoUb) with that of the frataxin wild-type. Calu-6 cells were transiently transfected with the plasmid encoding either His-frataxin or the mutant His-K^{147}R. At 24 h after the transfection, cells were treated with MG132 and lysed. His-tagged proteins were then tested for their ability to bind immobilized GST-tagged Ub protein. The purified GST and GST-monoUb were immobilized using glutathione (GSH) Sepharose beads and incubated with cell lysates containing the recombinant His-frataxin or the mutant His-K^{147}R. After binding, the proteins were eluted and analyzed by Western blotting with antibodies against the His epitope. Figure 3

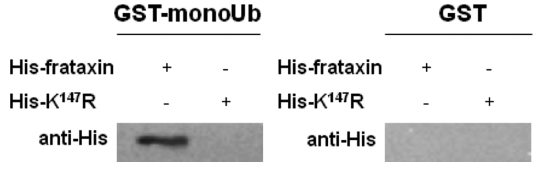

Figure 3. Analysis of the interaction between frataxin and Ub. Western blotting of GST pull-down experiments. Lysates from Calu-6 cells treated with MG132 for 18 h, overexpressing His-frataxin or His-K^{147}R, were pulled down with GST-monoUb or GST (control) as indicated. The eluted proteins were then immunoblotted with antibodies against the His epitope. These results are representative of three independently performed experiments.

shows that the signal for frataxin was present in the pull-down sample containing the wilde-type frataxin but not in that of

dx.doi.org/10.1021/jm3017199 | J. Med. Chem. 2013, 56, 2861–2873

the mutant His-$K^{147}R$, thereby confirming that K^{147} is essential for binding with Ub. The absence of a signal for frataxin in the pull-down preparation of GST confirmed the specificity of the assay.

Structural Model of the Frataxin-K^{147}/Ub Complex. A computational model of the frataxin/Ub complex was constructed considering the formation of a covalent isopeptide bond between the carboxyl group of the C-terminal G^{76} of Ub and the ε-NH_2 group of frataxin K^{147} with the help of the HADDOCK algorithm.[21] The coordinates for the mature human frataxin (residues 90−208) and Ub were taken from the current crystal structures[23,24] without modifications. The residues interacting across the frataxin-K^{147}/Ub complex interface were predicted by two interface prediction programs, WHISCY[25] and ProMate,[26] which generate the ambiguous interaction restraints (AIRs) (Table 1).

Table 1. List of Active and Passive Residues Used in the Definition of the AIRs for Docking of Frataxin and Ub

Frataxin (1EKG Chain A)	
active residues[a]	V144, Q148, P150, N151, W155, S157, P159, G162, P163, R165, Y175
passive residues[a]	E^{92}, V^{131}, T^{133}, G^{141}, T^{142}, K^{152}, S^{160}, S^{161}, D^{167}, S^{176}, H^{177}, D^{178}, G^{179}, V^{180}
Ub (1Q0W Chain B)	
active residues[a]	L^8, I^{44}, G^{47}, V^{70}
passive residues[a]	L^{71}, R^{72}, R^{74}
isopeptide bond (G^{76} of Ub to K^{147} of frataxin)[b]	unambiguous restraint distance (Å)
O−NZ	2.25 ± 0.05
C−NZ	1.35 ± 0.05
C−CE	2.45 ± 0.05
CA−NZ	2.45 ± 0.05

[a]The active and passive residues for the both protein partners were calculated by WHISCY Web server. Active residues are residues predicted to be involved in the interaction, and passive residues are their surface neighbors. [b]Ub and frataxin are connected via an isopeptide bond between the carbonyl C of G^{76} and the NZ atom of K^{147} (see Experimental Section).

Prediction programs identified L^8, I^{44}, G^{47}, and V^{70} as Ub active residues. Interestingly, they coincide with the residues known to form the hydrophobic patch involved in most of the monoUb/Ub-binding proteins interactions.[27,28] The predicted frataxin active residues V^{144}, Q^{148}, P^{150}, N^{151}, W^{155}, S^{157}, P^{159}, G^{162}, P^{163}, R^{165}, Y^{175}, located on the external surface of the β-sheet, match the amino acids highly conserved in all eukaryote and prokaryote sequences of frataxin (Table 1). The majority of these residues have no charge, making a flat and nearly neutral surface, suitable for mediating protein−protein interactions.

The covalent isopeptide bond between the G^{76} COOH group of Ub and the ε-NH_2 group of K^{147} was introduced using unambiguous distance restraints based on typical interatomic distances for a peptide bond in crystal structures, as described previously.[22] HADDOCK generated 200 structures, which were then subjected to clustering. Figure 4 shows a plot of the intermolecular energy, E_{inter}, of the 200 complex structures as a function of their backbone root-mean-square deviation (rmsd) from the lowest energy structure. After analysis, two clusters were obtained. Their statistical results are summarized in Table 2.

Cluster 1 of frataxin-K^{147}/Ub complex, containing 60 members, had the best average E_{inter} (−281.9 ± 103.1 kcal/mol). Likewise, all cluster evaluation parameters showed a significantly better performance of the best-scoring cluster 1 versus cluster 2. For

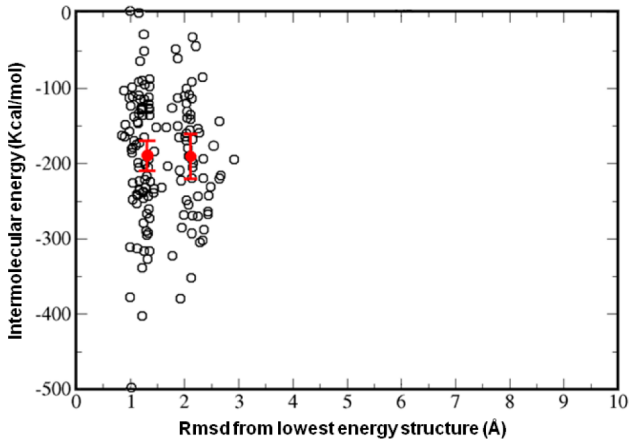

Figure 4. Intermolecular energies versus backbone rmsd at the interface from the lowest energy structure for the frataxin-K^{147}/Ub complex. Values for the single conformations (open circles) and cluster averages (filled red circles) are shown. The intermolecular energy corresponds to the sum of AIR, van der Waals, and electrostatic energy terms. Nonbonded energies were calculated according to OPLS parameters, using a 8.5 Å cutoff. Clustering was based on the pairwise backbone rmsd, using a 2.0 Å cutoff.

example, structures from the best-scoring cluster 1 showed the largest buried surface area (BSA) at the interface (1325 ± 94.8 Å), suggesting that solutions of the best-scoring cluster present sensible models for the Ub/frataxin interaction. Accordingly, the five lowest-energy structures of this cluster were selected for further analysis. As depicted in Figure 5, the structure of the complex is rather well-defined, with a backbone rmsd on interface of 0.51 ± 0.16 Å, and of good quality, with more than 96% of the residues in the most favored permitted regions of the Ramachandran plot (see Experimental Section).

A large number of intermolecular hydrophobic contacts were identified, together with a few H-bonds and salt bridges, the major one being between Ub R^{74} and frataxin D^{92}. The W^{155} side chain of frataxin, which points toward the center of the interacting surface of Ub, is in close contact with the Ub L^8, V^{70}, and L^{71} side chains. Moreover, the frataxin G^{141} α-H makes intimate contact with Ub G^{47}. Contribution to the stability of the complex also comes from the hydrophobic interactions between P^{163} and V^{144} of frataxin and I^{44}, L^8, and V^{70} of Ub. The three highly conserved frataxin residues W^{155}, P^{163}, and V^{144} seem to form a "trident" that anchors the frataxin domain to the hydrophobic patch of Ub, including L^8, I^{44}, G^{47}, and V^{70} residues (Figure 6). Notably, frataxin residue W^{155} and surrounding residues were shown to contribute to binding interactions with partner proteins and also to be important for frataxin function in Fe−S cluster biosynthesis.[29−32]

In Silico Screening of the Open NCI Library on Frataxin. With the goal of preventing frataxin/Ub association, we went on to search for small molecules capable of directly targeting the frataxin region that binds Ub. A multistep structure-based virtual screening of more than 65 000 leadlike compounds obtained from the NCI Open Database[33] was carried out. This is a large public database (260 071 compounds) from which sample compounds can be obtained through the NCI/Developmental Therapeutics Program. In order to focus the virtual screening on compounds suitable for further development, we selected a subset of leadlike compounds (referred in this work as the NCI leadlike set).[34,35] The selection was made based on properties and functional groups using the FILTER

dx.doi.org/10.1021/jm3017199 | J. Med. Chem. 2013, 56, 2861−2873

Table 2. Statistical Analysis of HADDOCK Results for the Generated Frataxin-K^{147}/Ub Complex after Clustering[a]

cluster[b]	rmsd E_{min} (Å)[c]	E_{inter} [d] (kcal/mol)	E_{wdw} [e] (kcal/mol)	E_{elec} [e] (kcal/mol)	E_{rest} [f] (kcal/mol)	E_{unamb} [g] (kcal/mol)	E_{amb} [h] (kcal/mol)	BSA[i] (Å^2)
cluster 1 [60]	1.14 ± 0.2	−281.9 ± 103.1	−57.3 ± 5.9	−256.6 ± 51.5	34.74 ± 6.7	0.02 ± 0.01	34.72 ± 6.7	1325 ± 94.8
cluster 2 [58]	2.13 ± 0.1	−236.7 ± 70.0	−20.0 ± 6.8	−251.7 ± 31.9	38.07 ± 5.6	0.04 ± 0.02	38.03 ± 5.6	1285 ± 86.5

[a]Clusters are sorted according to average intermolecular energy. [b]Sorting of the generated structures for frataxin-K^{147}/Ub complex into clusters. The corresponding cluster size is indicated in brackets. [c]Average rmsd and standard deviation from the lowest energy structure of all calculated structures. [d]Intermolecular energy: sum of the van der Waals and electrostatic energies. [e]Nonbonded energies were calculated with the OPLS parameters using a 8 Å cutoff. [f]Restraint energy: sum of unambiguous and ambiguous energies. [g]Unambiguous energy accounts for isopeptide-bond-related restraints. [h]Ambiguous energy accounts for restraints associated with interdomain contacts between the hydrophobic patch on Ub and the higly conserved residues on frataxin. [i]Total BSA: sum of the BSA for both frataxin and Ub subunities.

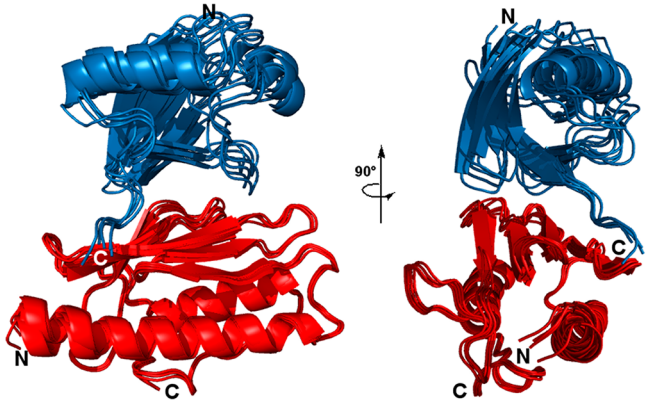

Figure 5. Ensemble of the five lowest-energy structures of the lowest-energy cluster of the frataxin-K^{147}/Ub complex. On the right side, the structures are viewed 90° from the orientation of those on the left side. Frataxin is shown in red and Ub in blue. Secondary structure elements are indicated. The figure was generated with Pymol (Delano Scientific LLC).

program[36] that reduced the initial NCI database to a subset of 65 375 compounds. After selection of leadlike compounds, a fast docking protocol was employed to further refine the NCI leadlike set. The general workflow of the multistep docking approach implemented in this work is presented in Figure 7. Structure-based screening was conducted using two docking programs, GLIDE[37] and AUTODOCK.[38] Consensus hits were selected and tested experimentally. Details of the workflow, screening compound numbers, and filters used for the virtual screening are reported in the Experimental Section.

In total, 25 consensus compounds with favorable docking scores were identified, and of these, 13 were selected for experimental testing based on 3D visualization and assessment in the frataxin/Ub interaction area, including the fit to the binding site shape, ligand conformation, and ability to form H-bonds with surrounding residues. The chemical structures of the selected hits are shown in Figure 8, while their docking scores and leadlike properties are available as Supporting Information.

The 13 compounds were tested for their ability to prevent the frataxin ubiquitination. To this aim, Calu-6 cells were transiently transfected with His-frataxin. At 24 h after the transfection, untransfected and transfected cells were treated with either 10 μM MG132 for 18 h or 100 μM of each selected molecule for 72 h. Untreated and treated cells were then harvested, and protein extracts were subjected to Western blotting analysis. All solutions were carefully monitored to avoid artifacts due to precipitation or agglomeration of compounds. Under assay conditions, aggregation

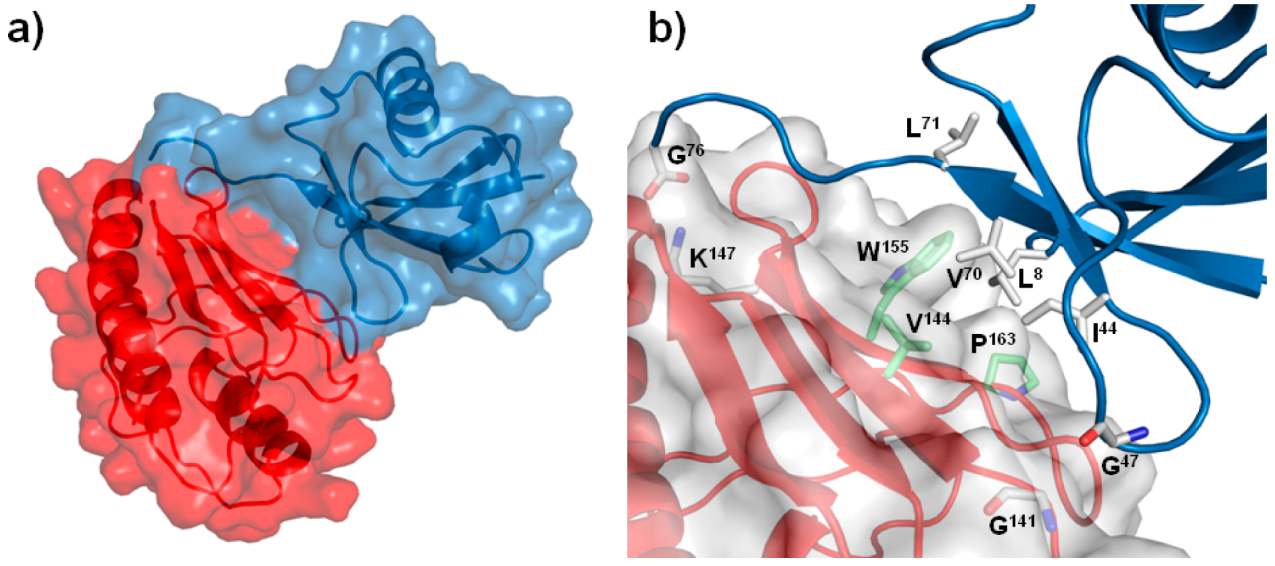

Figure 6. Frataxin/Ub interaction. (a) Surface representation of the frataxin-K^{147}/Ub complex. Frataxin and Ub are shown in semitransparent surfaces (red and blue, respectively) superimposed with their respective ribbon models. (b) Detailed view of the protein interface. Frataxin is shown in a surface representation superimposed with the ribbon model (red) and a stick model of residues interacting with Ub (white, carbon; blue, nitrogen; red, oxygen). Ub is shown as a ribbon model (blue) superimposed with a stick model of residues interacting with frataxin (white, carbon; blue, nitrogen; red, oxygen). The isopeptide linkage between the Ub G^{76} and frataxin K^{147} is displayed. The three highly conserved frataxin residues W^{155}, P^{163}, and V^{144} (green, carbon) form a "trident" that anchors the frataxin domain to the hydrophobic patch of Ub (L^{8}, I^{44}, G^{47}, and V^{70} residues).

dx.doi.org/10.1021/jm3017199 | J. Med. Chem. 2013, 56, 2861−2873

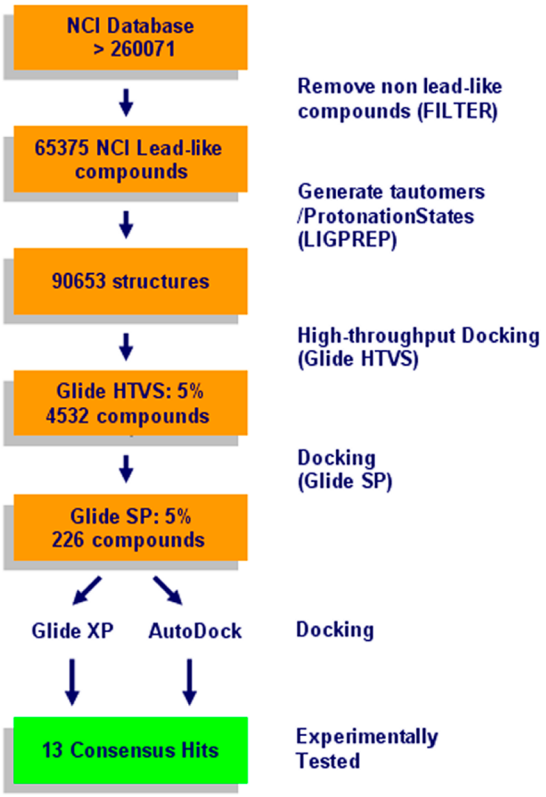

Figure 7. Flow chart of the multistep virtual screening strategy implemented in this work.

of active compounds was not detectable. In addition, none of these compounds had protein-reactive groups. Among the tested compounds, the (±)-6-((2,3-dimethoxyphenyl)(4-morpholinyl)-methyl)-1,3-benzodioxol-5-ol ((±)-**11**) was found to be the most effective in preventing the frataxin ubiquitination. Since compound **11** was tested as a racemic mixture, it was synthesized and resolved into its enantiomers (+)-**11** and (−)-**11**, which were assayed individually and compared to the racemate.

Synthesis and Resolution of Racemic Mixture of 11. Reaction between morpholine (**a**), 2,3-dimethoxybenzaldehyde (**b**), and benzo[*d*][1,3]dioxol-5-ol (**c**) resulted in the synthesis of (±)-**11** (Scheme 1). This reaction was studied under two conditions as follows: pathway A consisting of reflux in ethanol for 72 h; pathway B consisting of solvent-free microwave irradiation using CEM Discover S class microwave oven at 125 °C for 5 min in the absence of any catalyst.

Pathway A suffers from long reaction times up to several days and produces modest yields of product (about 47%) with a moderate enantiomeric excess (57%) for the (+)-isomer. On the contrary, the microwave-assisted solvent-free reaction (pathway B), a most efficient synthetic method in terms of energy and time consumption, furnishes better yields of the product (87%), with an equimolar presence of the two (+)- and (−)-enantiomers.

On the basis of these results, a hypothetical mechanism of reaction could be proposed to justify the different trend of the two pathways A and B (Scheme 2). In both synthetic methods, the secondary amine **a** attacks the carbonyl group of aldehyde **b**, yielding a racemic hemiaminale intermediate **H**. In pathway A, the electron poor carbon of **H** undergoes a S_N2 displacement by the carbon α to the phenol OH group of **c** to give a transition state with the geometry of a pentagonal bipyramid, probably stabilized by an intramolecular H-bond between the nitrogen of the morpholine and the phenol OH group. The formation of this six-membered H-bond could determinate a transient intermediate responsible for the excess of the (+)-isomer of **11**.

Under microwave irradiation (pathway B), a trigonal planar carbocation intermediate can be formed starting from **H**. The attack of phenol **c**, occurring on either face of the carbocation, yields the racemic mixture of **11**.

The most practical method for the resolution of racemic amines is the preparation of diastereomeric salts with an optically active acid and then separation via crystallization.[39] The resolution of (±)-**11** was accomplished through the sequential use of L- and D-tartaric acid (Scheme 3). When (±)-**11** and L-(+)-tartaric acid were used in a 1:0.5 ratio, (−)-**11** and (+)-**11** were isolated in 30% and 37% yields with >99% and 97% ee, respectively. In an optimized protocol, (±)-**11** and L-(+)-tartaric acid (0.5 equiv) were mixed in ethanol and stirred overnight. The solid tartrate salt was separated from the unreacted **11** through extraction with ether. Subsequent recrystallization of the salt from ethanol and basification gave (−)-**11**. The (+)-enantiomer was obtained from the mother liquor by similar treatment with D-(−)-tartaric acid. Both enantiomers were obtained in good yields and high enantiomeric purity after a single crystallization of the corresponding tartrate salts. The enantiomeric purity of both enantiomers was determined by chiral HPLC.

(+)-11 Promotes the Accumulation of Frataxin Precursor in Calu-6 Cells. Figure 9 shows the effect of 50 μM (±)-**11**, (+)-**11**, and (−)-**11** on the accumulation of precursor and mature frataxin in Calu-6 cells. In comparison with the racemate (±)-**11**, the isomer (+)-**11** indirectly induced a larger increase in the cellular concentration of mature frataxin by significantly restoring the endogenous level of frataxin precursor (Figure 9a). In contrast, (−)-**11** displayed no increase in the cellular concentration of frataxin, indicating a fine degree of selectivity in the binding site due to chiral geometry.

To verify that the increase of mature frataxin levels in cells is indeed due to the capacity of (+)-**11** to prevent the conjugation of Ub molecule with frataxin precursor, Calu-6 cells were transiently transfected with the plasmid encoding His-frataxin, and 24 h after the transfection, cells were treated with either 10 μM MG132 or 10 μM MG132 and 50 μM (+)-**11**. His-frataxin was then analyzed for its ability to bind to immobilized GST-monoUb. The purified GST and GST-monoUb were immobilized using GSH-Sepharose beads and incubated with the cell lysates treated or not with (+)-**11**. After the binding, the eluted proteins were analyzed by Western blotting with antibodies anti-His. Figure 9b shows that the signal for frataxin was present in the pull-down sample of untreated cells and absent in that of (+)-**11** treated cells, indicating that this compound is able to prevent the conjugation of Ub to frataxin precursor. Experiments conducted in Calu-6 cells with increasing compound concentrations showed a dose-dependent behavior of (+)-**11** in preventing the ubiquitination of frataxin (Figure S1 of Supporting Information). The IC_{50} for inhibition of frataxin ubiquitination was determined to be 45 μM. Cell viability was not impaired by (+)-**11** concentrations up to 100 μM.

Binding Affinity of Compound (+)-11 to Frataxin. To investigate the binding affinity of (+)-**11** with frataxin, we employed an UF-LC/MS based ligand-binding assay.[40,41] Initially in the binding assay experiments compound (+)-**11** (1 μM) was incubated at 25 and 37 °C with 1 μM for His-frataxin recombinant protein in a total volume of 200 μL of assay buffer. After the

dx.doi.org/10.1021/jm3017199 | J. Med. Chem. 2013, 56, 2861−2873

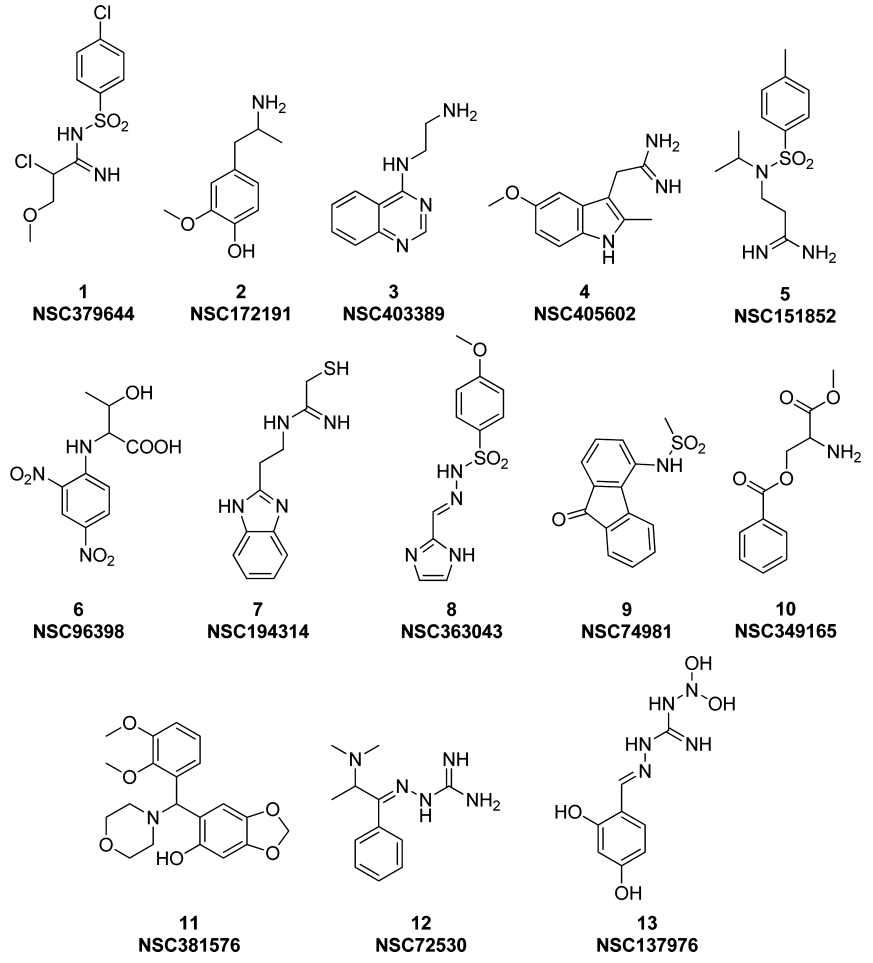

Figure 8. Chemical structures of compounds yielded by the multistep docking approach and tested experimentally.

Scheme 1. Synthesis of Compound (±)-11

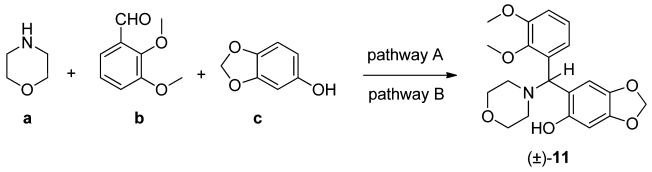

incubation, the unbound compound from the ligand–protein complex was removed by washing with assay buffer. Then the ligand was dissociated from the complex and analyzed by LC/MS. In the positive electrospray mass spectrum, the protonated molecule of compound (+)-**11** was detected at m/z 374.1598 $[M + H]^+$. Figure 10 shows the LC/MS analysis of an ultrafiltrate obtained from the incubation of test compound (+)-**11** with

Scheme 2

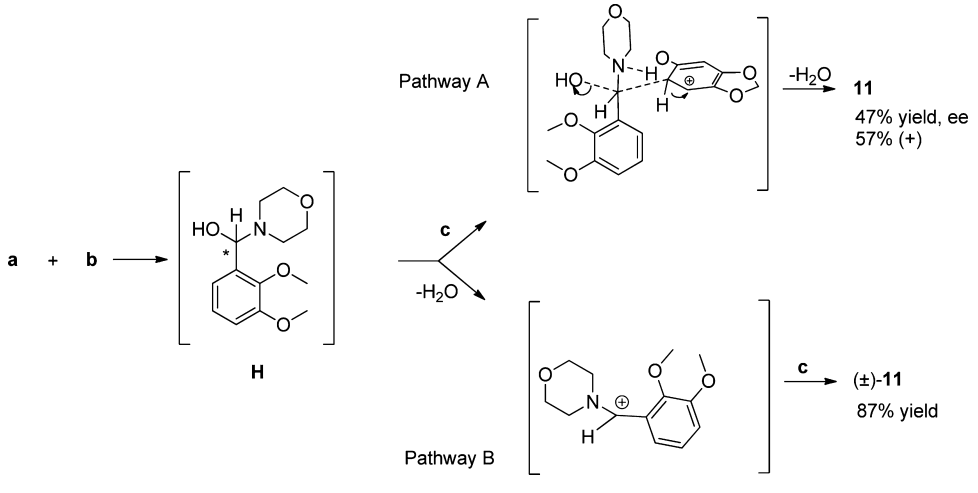

dx.doi.org/10.1021/jm3017199 | J. Med. Chem. 2013, 56, 2861–2873

Scheme 3. Resolution of (+)-11 and (−)-11 Enantiomers

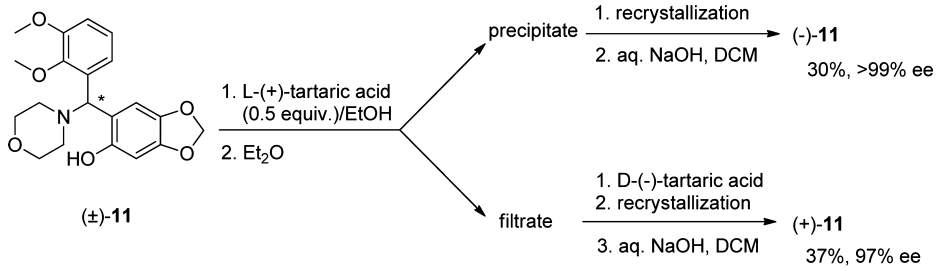

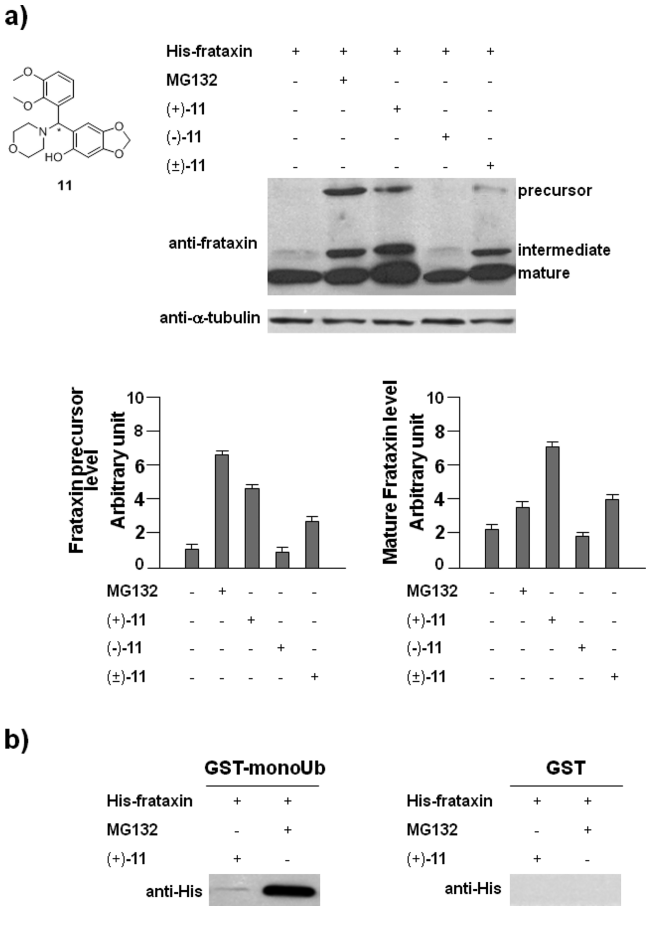

Figure 9. Effect of (±)-**11**, (+)-**11**, and (−)-**11** on human frataxin precursor and frataxin accumulation. (a) Western blot analysis with the indicated antibodies of protein extracts from Calu-6 cells transiently transfected with His-frataxin untreated and treated with 50 μM (±)-**11**, (+)-**11**, and (−)-**11** for 3 days or 10 μM MG132 for 18 h. The levels of proteins were quantified by PhosphorImager (Bio-Rad, Hercules, CA, U.S.) and normalized to tubulin levels. (b) Western blotting of GST pull-down experiments. Lysates from the same cells were pulled down with GST-monoUb or GST (control) as indicated. The eluted proteins were then immunoblotted with antibodies against the His epitope. These results are representative of three independently performed experiments.

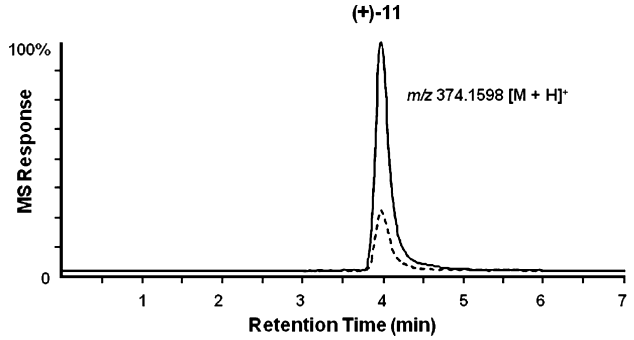

Figure 10. Ultrafiltration LC/MS screening of compound (+)-**11** incubated with 1 μM His-frataxin recombinant protein. Compound (+)-**11** was tested at 1 μM. The solid line represents the experiment using active frataxin protein, and the dotted line corresponds to the control incubation using denatured frataxin protein.

frataxin protein at 25 °C. The peak area of compound (+)-**11** was enhanced 3.70-fold in the chromatogram corresponding to the incubation with active frataxin compared to the control experiment carried out with denatured protein, which showed that compound (+)-**11** possesses specific binding affinity to frataxin. The peak area enhancement of (+)-**11** was 3.32-fold compared to control experiment when incubated at human body temperature of 37 °C. The relative binding affinity was ascertained by calculating the ratio between the average peak area of compound incubated with active protein and the average peak area of compound incubated with denatured protein. Our results show that (+)-**11** has specific binding affinity to frataxin. We attempted to investigate entropy and enthalpy changes by isothermal titration calorimetry, but these experiments unfortunately did not yield interpretable data (data not shown).

Although the absolute configuration of (+)-**11** is not known at the moment, we assume that it has *R* configuration, since docking calculations predicted the *R* enantiomer to bind more favorably to frataxin than the corresponding *S* enantiomer. We are currently attempting to crystallize the (+)-**11**/frataxin complex. Figure 11 illustrates a model of the (*R*)-**11**/frataxin complex as predicted by GLIDE. According to this model, residues V^{144}, N^{146}, W^{155}, S^{157}, G^{162}, P^{163}, and R^{165} form the binding pocket of (*R*)-**11**, and a network of H-bonds is predicted between the ligand and the side chains of N^{146}, S^{157}, and R^{165}. In particular, the meta methoxy oxygen of the phenyl ring of **11** forms bidentate H-bonds to the R^{165} side chain, while the OH oxygen of the benzodioxole system accepts a H-bond from the NH carboxamide of the N^{146} side chain. The morpholine oxygen atom is engaged in a H-bond with the S^{157} OH group. Furthermore, the ligand makes hydrophobic contacts with residues W^{155}, P^{163}, and V^{144}. Specifically, the dimethoxyphenyl ring and the benzodioxole aromatic ring of the ligand are oriented in such a way to establish parallel-displaced and T-shaped $\pi-\pi$ stacking interactions with the W155 side chain.

Scaffold Searching and SAR Development. Hierarchical screening is an efficient strategy allowing an initial broad search over a chemically and pharmacologically diverse set of compounds, followed by a focused search over a much larger database to find molecules related to potential lead compounds. The most promising compound **11** was selected for scaffold-searching and

dx.doi.org/10.1021/jm3017199 | J. Med. Chem. 2013, 56, 2861−2873

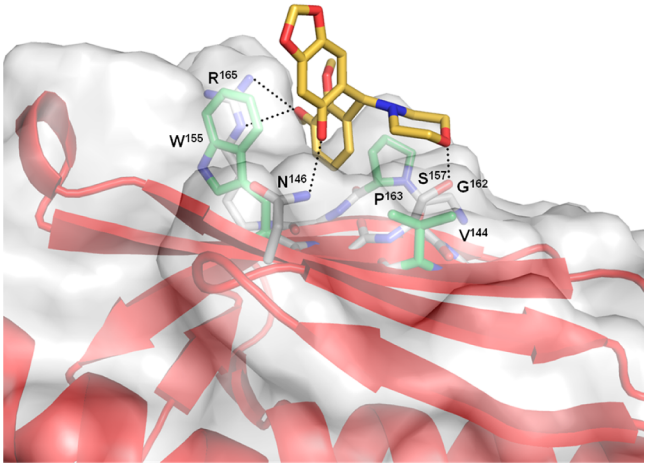

Figure 11. Binding mode of compound (*R*)-**11** (yellow) into the frataxin Ub-binding domain shown as a surface representation superimposed with the ribbon model (red). Only amino acids located within 3.5 Å of the ligand are shown and labeled. The highly conserved residues W^{155}, P^{163}, and V^{144} involved in Ub binding are displayed in green. H-bonds are indicated by dashed black lines.

SAR expansion studies. Substructure and similarity follow-up searches over the full NCI database resulted in 38 compounds matching the scaffold, which were docked to the frataxin Ub-binding site and ranked according to the predicted GLIDE XP/AUTODOCK consensus scoring. The top 12 compounds with the lowest scoring value for frataxin Ub-binding site were selected for experimental testing (Table 3). It was gratifying that they all showed a dose-dependent behavior in preventing the conjugation of Ub molecule to the precursor frataxin (Supporting Information Figure S1), confirming the viability of the core structure from **11**. Values of experimental IC_{50} (μM) for inhibition of frataxin ubiquitination were obtained as described in the Experimental Section. As previously, aggregation effects were excluded, and compound identity and purity were confirmed by elemental analysis and ^{1}H NMR (see Supporting Information).

As can be seen from data shown in Table 3, replacement of the morpholine ring with a piperidine (compound **23**) or pyrrolidine ring (compound **24**) led to a considerable reduction of activity. This is due to the loss of the H-bond between the morpholine oxygen and the OH group of S157. We observed a nearly 2-fold increase in inhibitory activity (from 45 to 20 μM) when the methoxy substituents were in meta and para positions of the phenyl ring (compound **15**), with a slight preference for the meta over the para position in this series (cf. compounds **18** and **14**). Compounds **14**, **16**, and **17**, lacking the meta methoxy substituent on the aromatic ring, were less potent than compound **11**. Docking of the two most active compounds **15** and **18** into the frataxin Ub-binding domain indicated that the oxygen atoms of the meta and para methoxy groups are optimally oriented to form two stable H-bonds to the R165 side chain (Supporting Information Figure S2).

We also observed that halogens (compounds **20** and **21**) and basic (compound **22**) substituents at the para position of the phenyl ring led to a nearly 1.5-fold decrease in activity over compound **11.** Finally, replacement of substituted phenyl ring with a benzodioxole system led to a drastic reduction in activity. From a visual inspection of compound **25** complexed to Ub-binding domain of frataxin, it seems clear that the presence of a second benzodioxole ring in the molecule increases the steric hindrance inside the binding cavity and changes the optimal binding mode of the ligand, thus decreasing the relative stability of the complex.

CONCLUSION

Here we describe our efforts in identifying novel small-molecule inhibitors that perturb conjugation of Ub onto frataxin. To this aim, we verified that treatment of Calu-6 cells with proteasome

Table 3. Structure and Activity of Compound 11 Scaffold Search Hits

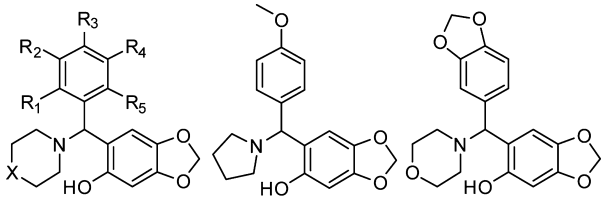

14-23 **24** **25**

compd	NSC no.	R_1	R_2	R_3	R_4	R_5	X	consensus score	QP log P [a]	IC_{50} (μM)[b]
14	364724	H	H	OCH_3	H	H	O	−11.41	1.91	65 ± 9.0
15	368252	H	OCH_3	OCH_3	H	H	O	−11.60	2.08	20 ± 4.0
16	381577	OCH_3	H	OCH_3	H	OCH_3	O	−9.28	2.31	53 ± 4.0
17	370277	OCH_3	H	OCH_3	H	H	O	−10.54	2.30	44 ± 9.0
18	368256	OH	OCH_3	H	H	H	O	−10.95	1.70	29 ± 4.0
19	667921	OH	H	H	H	H	O	−10.41	1.63	80 ± 9.0
20	368275	H	H	Cl	H	H	O	−10.94	2.55	68 ± 9.0
21	368277	H	H	F	H	H	O	−10.67	2.29	67 ± 5.0
22	368269	H	H	$N(CH_3)_2$	H	H	O	−10.14	2.42	81 ± 9.0
23	368274	H	H	OCH_3	H	H	C	−10.38	3.10	82 ± 5.0
24	370281							−10.06	2.96	97 ± 12.0
25	368248							−10.12	1.64	70 ± 9.5
(+)-**11**	381576	OCH_3	OCH_3	H	H	H	O	−11.13	2.41	45 ± 6.0

[a]Predicted octanol/water partition coefficient using the QikProp 3.4 program [50]; range of recommended values (−2.0)-(+6.5). [b]IC_{50} values are the means ± SEM of a series separate assays, each performed in triplicate.

dx.doi.org/10.1021/jm3017199 | *J. Med. Chem.* 2013, 56, 2861−2873

inhibitors (MG132 and bortezomib) led to a significant accumulation of frataxin precursor and, indirectly, of its mature form, thereby confirming the role of the UPS in the degradation pathway of frataxin. Site-directed mutagenesis experiments showed that K^{147}/R mutant of frataxin completely failed to conjugate Ub, suggesting that this lysine residue is its target site for Ub conjugation. With the help of the protein−protein docking program HADDOCK, we built a computational model of the frataxin-K^{147}/Ub complex. A small molecule (compound (±)-**11**) targeting the Ub-binding domain of frataxin was identified by a multistep structure-based virtual screening. This chiral compound was synthesized and resolved in its optical isomers. (+)-**11** was the active isomer capable of blocking the frataxin ubiquitination and of promoting the accumulation of both precursor and mature frataxin species in Calu-6 cells. The binding affinity of (+)-**11** for frataxin was investigated through the UF-LC/MS based ligand-binding assay. The peak area of the ligand in the chromatogram corresponding to incubation with active frataxin increased by 3.70-fold compared to the chromatogram of test compound incubated with denatured protein, thus revealing the existence of a specific interaction between (+)-**11** and frataxin. A docking model elucidating the putative interactions between compound **11** and frataxin Ub-binding site is proposed. On the basis of this model, it can be hypothesized that compound **11** could mask the residues required for Ub interaction or mask a putative sequence containing some form of signal that is recognized by Ub machinery. Substructure and similarity follow-up searches on the most active hit compound **11** yielded a series of morpholino analogues with a key meta and para methoxy substituted phenyl ring that possessed activity in the micromolar range.

In conclusion, by combining theoretical and experimental approaches, we identified a small molecule that disrupts the frataxin/Ub interaction determining a half-life increase of cellular frataxin. This finding is very significant because the increment in the residual levels of frataxin could open therapeutic perspectives for the FRDA disease.

■ EXPERIMENTAL SECTION

Interface Prediction. The X-ray coordinate files of human frataxin (PDB code 1EKG, chain A)[23] and Ub (PDB code 1UBQ)[24] were downloaded from the PDB,[42] while the multiple sequence alignments were taken from the HSSP database (ftp://ftp.cmbi.kun.nl/pub/molbio/data/hssp).[43] The first aligned sequence in the HSSP file was taken as master sequence. WHISCY[25] and ProMate[26] were used for interface predictions and combined for consensus scoring using WHISCYMATE.[25] Multiple sequence alignments were used for WHISCY prediction: if there was any disagreement between structure and master sequences about a residue identity, the residue of the master sequence was used. The parts of a structure that were not present in the alignment were not predicted and ignored in the evaluation. ProMate predictions were obtained making use of the Web interface of ProMate (http://bioinfo.weizmann.ac.il/promate/promate.html) using default settings. For WHISCYMATE, a residue was predicted if its ProMate score was higher than or equal to 98.520, its WHISCY score higher than or equal to 0.371, or its ProMate and WHISCY scores were both higher than or equal to 55.420 and 0.107, respectively. Interface predictions were used to generate AIRs as discussed before:[25] predicted residues were designated active residues and their surface neighbors passive residues (Table 1).

Docking for the Frataxin-K^{147}/Ub Complex. A structural model of frataxin-K^{147}/Ub complex was obtained following a WHISCY-HADDOCK docking approach.[21,22] The crystal structures of the human frataxin[23] and Ub[24] were used for mapping the interfaces and docking the structures. The restraints that were used in this study are listed in Table 1. Ub and frataxin were linked to one another via a G^{76}-K^{147} isopeptide bond. To account for the possible close contact between the hydrophobic patch on Ub (residues L^8, I^{44}, G^{47}, and V^{70}) and the highly conserved residues on the frataxin external surface, we incorporated AIRs where active and passive residues on both Ub and frataxin were defined exploiting the interface prediction WHISCY program.[25] The G^{76}-K^{147} isopeptide bond was modeled by including a set of distance restraints based on typical interatomic distances for a peptide bond in crystal structures, as described previously.[22] Backbone and side chain flexibility was also included to account for a possible conformational rearrangement that could occur at the interface between both Ub and frataxin moieties (Table 1). Flexible segments were defined as stretches of active and passive residues plus one sequential neighbor. The docking calculations were performed with the standard HADDOCK protocol as described by Dominguez et al.[21] For each run, 1000 rigid-body docking solutions were first generated by energy minimization. The driving force for the docking at this stage comes mainly from the AIRs and from van der Waals and electrostatic energy terms once the structures are within the nonbonded cutoff (8.5 Å). The 200 best solutions according to the AIR restraint energy (as defined in ref 21) were subjected to semiflexible simulated annealing in torsion angle space followed by a final refinement in explicit water.[44] During the simulated annealing and the water refinement, the amino acids at the interface (side chains and backbone) are allowed to move to optimize the interface packing. The nonbonded energies were calculated with the OPLS parameters[45] using a 8.5 Å distance cutoff. A dielectric constant of 10 was chosen for the vacuum stages of the docking protocol (rigid-body and semiflexible refinement).

The resulting structures were finally subjected to a final refinement in explicit water, clustered using a 2.0 Å backbone rmsd cutoff criterion, and sorted according to the intermolecular energy (sum of the van der Waals, electrostatic, and AIRs energy). BSA was calculated by taking the difference between the sum of the solvent-accessible surface area for each partner separately and the solvent-accessible area of the complex. The solvent-accessible area was calculated using a 1.4 Å water probe radius. The five best structures of the lowest energy cluster of each HADDOCK run were analyzed in terms of intermolecular contacts, and an average structure was calculated by superimposing the structures on the backbone atoms of the flexible segments. The Ramachandran plot of the generated model shows 71.7% of the residues in the most favored regions, 24.9% in the additional allowed regions, 1.1% in the generously allowed region, and 2.3% in the disallowed regions. Intermolecular contacts (H-bonds and nonbonded contacts) were analyzed with DIMPLOT, which is part of the LIGPLOT software, using the default settings (3.9 Å heavy-atoms distance cutoff for nonbonded contacts; 2.7 and 3.35 Å proton−acceptor and donor−acceptor distance cut-offs, respectively, with minimum 90° angles [D−H−A, H−A−AA, D−A−AA] for hydrogen bonds).[46]

Protein Preparation. The X-ray coordinates of human frataxin[23] were prepared using the Protein Preparation Wizard implemented in the Schrodinger package using default options: bond orders were assigned, hydrogens were added, and all water molecules were deleted. Hydrogens were then optimized using the exhaustive sampling option, and the protein was minimized to an rmsd limit from the starting structure of 0.3 Å using the Impref module of Impact with the OPLS_2005 force field.

Database: Leadlike Selection and Preparation. The NCI Open Database[33] with 260 071 compounds was obtained from ZINC.[47] The compound database was processed with FILTER,[36] version 2.0.1, to select a subset of leadlike compounds. We used the default parameters in the leadlike filter without further modifications. The resulting database contained 65 375 compounds. For docking, different protonation states and tautomers were generated with the GLIDE module LIGPREP. This yielded a total of 90 653 structures.

Docking with GLIDE and AUTODOCK. We employed the high-throughput virtual screening (HTVS) docking mode in GLIDE,[37] version 5.7, for a rapid structure-based filtering of the NCI leadlike set. This data set was docked onto the putative frataxin Ub-binding domain. The grid-enclosing box, which must contain the center of each ligand docked, was centered on the W^{155} side chain and defined to enclose residues located within 14 Å from W^{155}, while the outer box,

dx.doi.org/10.1021/jm3017199 | J. Med. Chem. 2013, 56, 2861−2873

in which all parts of the ligand must bind, was 35 Å in each direction. A van der Waals radius scaling factor of 0.80 for atoms with a partial atomic charge (absolute value) less than 0.15 was used in order to soften the potential for nonpolar parts of theprotein. Next, a flexible docking with default parameters was employed for virtual screening. The general workflow of the multistep docking approach implemented is depicted in Figure 7. The top-ranked compounds with GLIDE HTVS (4532 unique molecules) were docked flexibly in a stepwise manner with GLIDE Standard Precision (SP) and Extra Precision (XP). We employed default parameters with the same receptor grids used with GLIDE HTVS. Selected compounds docked with GLIDE XP (226 unique molecules) were also docked with AUTODOCK,[38] version 4.2. We used the same grid maps (centered on W^{155} residue) and default docking parameters. The only modification was the number of docking runs that was set to 10 for faster virtual screening. A consensus score was generated by combining both the AUTODOCK binding energy and the XP GLIDE score energy in order to increase confidence in the resulting energy score. High ranking poses by two different scoring functions represent, by construction, a more reliable prediction than any of the constituent scoring functions alone. In practice, consensus scoring has been generally found to improve virtual screening performance dramatically with respect to the individual scoring functions.[48,49] Out of the final 50 compounds identified from the multistep docking approach, 13 (Figure 8) were selected for experimental testing. The program QikProp,[50] version 3.4, was used for calculating the ADME proprieties.

Scaffold Search. An online search utility provided by the NCI (http://129.43.27.140/ncidb2/)[51] was used to search the entire NCI database for compounds similar to compound **11**. Two methods were used to judge compound similarity: search on the basis of substructure by SMILES string (http://daylight.com) and similarity by Tanimoto coefficient,[52] with a cutoff of 0.85.[53] From these searches, selected compound structures were docked to the frataxin Ub-binding site and ranked according to predicted GLIDE XP/AUTODOCK consensus scoring. Compounds with the lowest scoring value were requested and assayed for effect on frataxin ubiquitination.

General Procedures. Reagents, starting material, and solvents were purchased from commercial suppliers and were used as received. Analytical TLC was performed on a 0.25 mm layer of silica gel 60 F254 from Merck, and preparative TLC was performed on 20 × 20 cm^2 glass plates coated with a 2 mm layer of silica gel PF254 from Merck. Silica gel 60 (300−400 mesh), Merck, was used for flash chromatography. Melting points were taken on a Kofler apparatus and are uncorrected. Optical rotations were determined with a Perkin-Elmer 241 MC polarimeter. ^{1}H NMR spectra were recorded with a Bruker 500 spectrometer. Chemical shifts are reported in δ relative to internal Me_4Si, and J values are reported in Hz. Electrospray mass spectra were recorded using a WATERS Z-Q mass spectrometer equipped with an electrospray ionization (ESI) probe operating in positive or negative ion mode. CEM Discover S class microwave reactor was used for the microwave-assisted reactions.

Synthesis of 6-((2,3-Dimethoxyphenyl)(4-morpholinyl)-methyl)-1,3-benzodioxol-5-ol ((±)-11). Morpholine (**a**), 2,3-dimethoxybenzaldehyde (**b**), and benzo[*d*][1,3]dioxol-5-ol (**c**) were combined, and two reaction conditions were employed.

Pathway A. **a** (870 μL, 10 mmol), **b** (1.66 g, 10 mmol), and **c** (1.38 g, 10 mmol) were dissolved in ethanol (40 mL) and refluxed for 72 h. After the reaction proceeded for the stated period of time, a mass of colorless crystals separated. These were collected and recrystallized from acetone/methanol to give 1.75 g of **11** (yield 47%). Mp (°C): 141−142. ^{1}H NMR (500 MHz, $CHCl_3$-d_1) δ 7.32−762 (m, 3H), 6.43 (s, 1H), 6.38 (s, 1H), 5.82 (d, J = 1.0 Hz, 1H), 5.78 (d, J = 1.0 Hz, 1H), 4.96 (s, 1H), 3.90 (s, 3H), 3.83 (s, 3H), 3.70 (m, 4H), 2.52 (m, 4H). ESI-MS: 374 $(M + H)^+$. Anal. Calcd for $C_{20}H_{23}NO_6$: C 64.33, H 6.21, N 3.75. Found: C 64.41, H 6.26, N 3.80.

Pathway B. A mixture of **a** (87 μL, 1 mmol), **b** (166 mg, 1 mmol), and **c** (138 mg, 1 mmol) was mixed in a 50 mL flask and irradiated in a CEM Discover S class microwave oven at 125 °C for 10 min in the absence of any catalyst. The progress of the reaction was monitored with TLC. After cooling, the mixture was extracted with chloroform. Evaporation of the solvent under reduced pressure gave the crude product, which was recrystallized from acetone/methanol to give 324 mg of **11** (yield 87%).

Resolution of (±)-11. To a solution of L-(+)-tartaric acid (0.15 g, 1.0 mmol) in ethanol (3 mL) was added a solution of (±)-**11** (1.5 g, 4 mmol) in ethanol (15 mL), and the resulting mixture was stirred overnight at room temperature. Ethanol was then removed on a rotary evaporator at 40 °C. To the residue, diethyl ether (10 mL) was added, and the mixture was stirred for 1 h. Filtration of the reaction mixture provided the tartrate salt, which was recrystallized from ethanol (10 mL) to obtain white crystals. This solid was treated with aqueous NaOH solution, then extracted with CH_2Cl_2, dried over Na_2SO_4 and the solvent removed under reduced pressure to afford a white powder 0.21 g (yield 30%), mp 141−142 °C. The enantiomeric purity was determined by chiral HPLC (Daicel Chiralcel OD-H, hexane/isopropanol = 97.5:2.5, flow rate 1.0 mL/min) and was found to be >99%, $[\alpha]_D^{25}$ −171.4 (*c* 0.42, CH_2Cl_2). The second isomer of **11** was isolated from the mother liquor and treated with D-(−)-tartaric acid in ethanol as described above, providing the corresponding (+)-enantiomer, 0.27 g (yield 37%); mp 139−140 °C; $[\alpha]_D^{25}$ +151.2 (*c* 0.39, CH_2Cl_2). The enantiomeric purity was determined by chiral HPLC and was found to be 97%.

Cell Cultures, Constructs, and Transfections. The human lung carcinoma Calu-6 cell line (ATCC, HTB 56; ICLC, HTL97003) was cultured in Dulbecco's modified Eagle medium (DMEM) with Glutamax (Invitrogen, Carlsbad, California) supplemented with 10% fetal bovine serum (FBS), 2 mM L-glutamine, 50 U/mL penicillin−streptomycin, and 0.1 mM nonessential amino acids. Plasmids were transfected in Calu-6 cell line by using LIPOTAXI (Agilent) according to the manufacturer's instructions. Transfection efficiency was assessed by co-transfecting a GFP-expressing vector and normalizing RNA levels against GFP mRNA levels (data not shown). Where indicated, 24 h after transfection, cells were treated either with 10 μM proteosome inhibitors (MG132, bortezomib) for 18 h or with 100 μM of each of the 13 molecules selected by the multistep docking approach for 72 h. Then proteins were extracted and analyzed by Western blotting.

DNA Constructs and Production of Recombinant Proteins. The cDNA of frataxin was obtained by RT-PCR from cells using the primers forward 5′-TATGTGGACTCTCGGGCG-3′ and reverse 5′-TAGCATCTTTTCCGGAATAGG-3′ and cloned into the eukaryotic expression vector pcDNA3.1 H/Myc C (Invitrogen) and prokaryotic expression vector pRSET-A (Invitrogen). The cDNA of mutated frataxin containing R^{147} for K^{147} was generated using the QuikChange Lightning site-directed mutagenesis kit (Stratagene, catalog no. 210518) using the primers forward 5′-ATGTGATCAACA**G**G-CAGACGCCAAACAAG-3′ and reverse 5′-CTTGTTTG-GCGTCTGC**C**TGTTGATCACA-3′ and cloned into the prokaryotic expression vector pRSET-A to obtain the His-K^{147}R construct. The cDNA of human Ub (a gift from Dr. V. Colantuoni) was cloned in the prokaryotic expression vector pGEX4T3 (GE Healthcare, Waukesha, WI). The recombinant proteins GST-monoubiquitin and GST were expressed in *Escherichia coli* and purified by using glutathione Sepharose 4B beads according to the manufacturer's instructions (GE Healthcare). The recombinant proteins His-frataxin and His-K^{147}R were expressed in *E.coli* and purified by nickel nitrilotriacetic acid (Ni-NTA)−agarose chromatography according to the manufacturer's instructions (Qiagen, Valencia, CA).

Chemicals. All compounds were kindly provided by NCI (http://dtp.cancer.gov). The identity and purity of the assayed compounds were independently assessed by elemental analysis and ^{1}H NMR (see Supporting Information). Proteasome inhibitors MG132 and bortezomib were from Sigma-Aldrich and Santa Cruz Biotechnology, respectively.

Immunoprecipitation and Western Blotting. For immunoprecipitation assay, an amount of 1.5 mg of cell extracts was incubated with 20 μL of protein A/G agarose beads coated with 5 μL of antibody against frataxin (Millipore) at 4 °C for 12 h. The beads were washed and boiled in the SDS sample buffer. The eluted proteins were loaded on 12% SDS−PAGE and detected by Western blotting. Aliquots of protein samples (50 μg) were resolved by 15% SDS−gel electrophoresis and transferred into nitrocellulose filters. The membranes

were blocked in PBS, 0.1% Triton, and 5% dry milk for 2 h and then challenged with anti-frataxin (Millipore). The proteins were visualized with enhanced chemiluminescence detection reagent according to the manufacturer's instructions (Pierce, Rockford, Illinois).

Ubiquitination Assay and GST Pull-Down. For Ub assay, Calu-6 cells were transiently transfected with plasmids encoding His-frataxin or His-$K^{147}R$. At 24 h after transfection, cells were treated with 10 μM proteosomal inhibitor MG132 dissolved in DMSO for 18 h or with 50 μM (+)-**11** for 3 days and MG132 in the last 18 h. Then cells were harvested and lysed for 10 min on ice in lysis buffer (50 mM HEPES, 150 mM NaCl, 1 mM EDTA, 1 mM EGTA, 10% glycerol, 1% Triton-X-100, 25 mM NaF, 10 μM $ZnCl_2$, pH 7,5) containing protease inhibitor 1× (Roche). Cell lysates were then collected and centrifuged for 15 min at 13000*g*. An amount of 500 μg of the soluble fraction was incubated with 5 μg of GST-monoUb or GST coupled to glutathione Sepharose 4B (Amersham Biosciences, Frieburg, Germany) in pull-down buffer (50 mM Tris-HCl, pH 7.5, 0.4 mM EDTA, 150 mM NaCl, 10% glicerol, 1% NP-40, 1 mM sodium orthovanadate, 50 mM NaF, 5 mM DTT, and protease inhibitor mix 1×) for 4 h at 4 °C. After incubation, the beads were washed three times with lysis buffer. Eluted proteins were loaded on 12% SDS−PAGE and analyzed by immunoblotting using anti-His antibodies. Band intensities of ubiquitinated frataxin were quantified by densitometry scanner analysis (Bio-Rad, Hercules, CA, U.S.), and relative values are shown as percentage of control. Each data point represents the mean ± SEM of at least three independent experiments. The IC_{50} values were calculated using a four-parameter logistical model of the graph of log of dose against percentage of ubiquitinated frataxin values.

UF-LC/MS Based Frataxin Binding Assay. The test compound (+)-**11** (1 μM in 4 μL of DMSO) and 185 μL of assay buffer consisting of 100 mM Tris-HCl (pH 7.5), 50 mM KCl, and 5 mM $MgCl_2$ were placed into a microcentrifuge tube and incubated for 2 min at 25 °C. The binding assay was initiated by the addition of 1 μM His-frataxin recombinant protein and incubated further for 60 min at 25 °C. After incubation the binding mixture was filtered through an ultramembrane filter (Microcon YM-10, Millipore, Billerica, MA) according to the modified method of Nikolic et al.[40] and centrifuged at 13000*g* for 20 min at 4 °C. The protein−ligand complex was treated with assay buffer (200 μL × 3) and centrifuged at 13000*g* for 20 min at 4 °C to remove the unbound ligand. The ultramembrane filter was then placed into a new microcentrifuge tube, and the protein−ligand complex was allowed to stand in 200 μL of methanol for 20 min to dissociate the ligand completely. The content was then centrifuged at 13000*g* for 20 min at 20 °C. The ultracentrifugate was dried under nitrogen (NVAP 116 nitrogen evaporator, Organomation Associates, Inc., Berlin, MA). The sample was reconstituted in 100 μL of 50% methanol in deionized water (v/v) and analyzed by LC/MS. A control experiment was carried out in a similar manner with denatured His-frataxin protein. Prior to the assay, the protein was denatured by heating at 90 °C for 1 h. The test compound (+)-**11** was prepared in DMSO. The concentration of DMSO in the assay never exceeded 2% (v/v), a concentration that was found not to influence the results of the assay. The binding experiments for compound (+)-**11** (1 μM) against 1 μM His-frataxin protein were carried out at 25 and 37 °C to evaluate the influence of temperature. All the binding assays were performed in duplicate and analyzed twice.

LC/MS Analysis of Compound (+)-11. Analysis of (+)-**11** was carried out using an Agilent (Little Falls, DE) 6520 Accurate-Mass Q-TOF mass spectrometer equipped with an Agilent 1200 RRLC system. Chromatographic analysis of (+)-**11** was carried out using ZORBAX Eclipse plus C18 column (2.1 mm × 100 mm, 1.8 μm). The gradient solvent systems used were solvent A (95% water/5% methanol/0.1% acetic acid, v/v) and solvent B (0.1% acetic acid in methanol, v/v). The linear gradient was increased from 50% to 100% B in 5 min. The mobile phase was maintained with 100% B up to 6 min and then returned to the initial conditions of 50% B in 7 min. The column was equilibrated with 50% B for 5 min. The flow rate was 0.2 mL/min, and the injection volume for all samples was 2 μL. Nitrogen was supplied as nebulizing and drying gas at flow rates of 30 and 480 L/h, respectively. The drying gas temperature was 350 °C. The ESI source was operated with a capillary voltage of 3200 V. The fragmentor voltage was optimized to 175 eV. The released ligand (2 μL) was subjected to LC/MS analysis with a flow rate of 0.2 mL/min.

■ ASSOCIATED CONTENT

Ⓢ Supporting Information

Elemental analysis and ^{1}H NMR data of compounds **14**−**25**; dose−response behavior of compound (+)-**11** and its analogues **14**−**25**; binding modes of compounds **15** and **18** into the frataxin Ub-binding domain (PDF); results of in silico screen for the 226 top-ranked structures from NCI Open Database (XLS). This material is available free of charge via the Internet at http://pubs.acs.org.

■ AUTHOR INFORMATION

Corresponding Author

*Phone: +39-081-678613. Fax: +39-081-678012. E-mail: lavecchi@unina.it.

Author Contributions

All authors have given approval to the final version of the manuscript.

Notes

The authors declare no competing financial interest.

■ ACKNOWLEDGMENTS

This work was financially supported by the Ministero dell'Istruzione, dell'Università e della Ricerca Scientifica e Tecnologica (MIUR-PRIN 2010-2011, prot. 2010W7YRLZ_003), Rome, Italy. Gratitude is expressed to the National Cancer Institute for providing test compounds free of charge. The authors are grateful to the Centro Interdipartimentale di Metodologie Chimico-Fisiche CIMCF and the Centro Interdipartimentale di Analisi Strumentale dell'Università di Napoli "Federico II". The authors thank Prof. Adele Bolognese for thoughtful contributions and critical reading of the manuscript.

■ ABBREVIATIONS USED

AIR, ambiguous interaction restraint; BSA, buried surface area; Calu-6, human pulmonary carcinoma cell line; DMSO, dimethyl sulfoxide; DTT, dithiothreitol; EDTA, ethylene glycol tetraacetic acid; EGTA, ethylenediaminetetraacetic acid; FRDA, Friedreich's ataxia; GSH, glutathione; GST, glutathione *S*-transferase; HA tag, hemagglutinin; HADDOCK, high ambiguity driven protein−protein docking; His tag, 6-histidine; His, histidine; HPLC, high-performance liquid chromatography; HTVS, high-throughput virtual screening; MG132, *N*-carbobenzoxyl-L-leucinyl-L-leucinyl-L-leucinal; NCI, National Cancer Institute; PBS, phosphate buffered saline; PDB, Protein Data Bank; rmsd, root-mean-square deviation; SDS−PAGE, sodium dodecyl sulfate−polyacrylamide gel electrophoresis; Ub, ubiquitin; UF-LC/MS, ultrafiltration liquid chromatography/mass spectrometry; UPS, ubiquitin proteasome system

■ REFERENCES

(1) Harding, A. E. Classification of the hereditary ataxias and paraplegias. *Lancet* **1983**, *1*, 1151−1155.

(2) Campuzano, V.; Montermini, L.; Molto, M. D.; Pianese, L.; Cossee, M.; Cavalcanti, F.; Monros, E.; Rodius, F.; Duclos, F.; Monticelli, A.; Zara, F.; Canizares, J.; Koutnikova, H.; Bidichandani, S. I.; Gellera, C.; Brice, A.; Trouillas, P.; De Michele, G.; Filla, A.; De Frutos, R.; Palau, F.; Patel, P. I.; Di Donato, S.; Mandel, J. L.; Cocozza, S.; Koenig, M.; Pandolfo, M. Friedreich's ataxia: autosomal recessive

disease caused by an intronic GAA triplet repeat expansion. *Science* **1996**, *271*, 1423−1427.
(3) Delatycki, M. B.; Williamson, R.; Forrest, S. M. Friedreich ataxia: an overview. *J. Med. Genet.* **2000**, *37*, 1−8.
(4) Pandolfo, M. Friedreich ataxia: detection of GAA repeat expansions and frataxin point mutations. *Methods Mol. Med.* **2006**, *126*, 197−216.
(5) Patel, P. I.; Isaya, G. Friedreich ataxia: from GAA triplet-repeat expansion to frataxin deficiency. *Am. J. Hum. Genet.* **2001**, *69*, 15−24.
(6) Harding, A. E. Friedreich's ataxia: a clinical and genetic study of 90 families with an analysis of early diagnostic criteria and intrafamilial clustering of clinical features. *Brain* **1981**, *104*, 589−620.
(7) Harding, A. E. Clinical features and classification of inherited ataxias. *Adv. Neurol.* **1993**, *61*, 1−14.
(8) De Michele, G.; Filla, A.; Cavalcanti, F.; Di Maio, L.; Pianese, L.; Castaldo, I.; Calabrese, O.; Monticelli, A.; Varrone, S.; Campanella, G.; Leone, M.; Pandolfo, M.; Cocozza, S. Late onset Friedreich's disease: clinical features and mapping of mutation to the FRDA locus. *J. Neurol., Neurosurg. Psychiatry* **1994**, *57*, 977−979.
(9) Sakamoto, N.; Ohshima, K.; Montermini, L.; Pandolfo, M.; Wells, R. D. Sticky DNA, a self-associated complex formed at long GAA*TTC repeats in intron 1 of the frataxin gene, inhibits transcription. *J. Biol. Chem.* **2001**, *276*, 27171−27177.
(10) Pandolfo, M. Frataxin deficiency and mitochondrial dysfunction. *Mitochondrion* **2002**, *2*, 87−93.
(11) Pandolfo, M. Friedreich Ataxia and Related RNA Loss-of-Function Disorders. In *Molecular Neurology*, 1st ed.; Waxman, S., Ed.; Elsevier Academic Press: San Diego, CA, 2007; pp 277−294.
(12) Condò, I.; Ventura, N.; Malisan, F.; Rufini, A.; Tomassini, B.; Testi, R. In vivo maturation of human frataxin. *Hum. Mol. Genet.* **2007**, *16*, 1534−1540.
(13) Schmucker, S.; Argentini, M.; Carelle-Calmels, N.; Martelli, A.; Puccio, H. The in vivo mitochondrial two-step maturation of human frataxin. *Hum. Mol. Genet.* **2008**, *17*, 3521−3531.
(14) Cavadini, P.; Adamec, J.; Taroni, F.; Gakh, O.; Isaya, G. Two-step processing of human frataxin by mitochondrial processing peptidase. Precursor and intermediate forms are cleaved at different rates. *J. Biol. Chem.* **2000**, *275*, 41469−41475.
(15) Koutnikova, H.; Campuzano, V.; Koenig, M. Maturation of wild-type and mutated frataxin by the mitochondrial processing peptidase. *Hum. Mol. Genet.* **1998**, *7*, 1485−1489.
(16) Acquaviva, F.; De Biase, I.; Nezi, L.; Ruggiero, G.; Tatangelo, F.; Pisano, C.; Monticelli, A.; Garbi, C.; Acquaviva, A. M.; Cocozza, S. Extra-mitochondrial localisation of frataxin and its association with IscU1 during enterocyte-like differentiation of the human colon adenocarcinoma cell line Caco-2. *J. Cell Sci.* **2005**, *118*, 3917−3924.
(17) Condò, I.; Ventura, N.; Malisan, F.; Tomassini, B.; Testi, R. A pool of extramitochondrial frataxin that promotes cell survival. *J. Biol. Chem.* **2006**, *281*, 16750−16756.
(18) Lu, C.; Cortopassi, G. Frataxin knockdown causes loss of cytoplasmic iron−sulfur cluster functions, redox alterations and induction of heme transcripts. *Arch. Biochem. Biophys.* **2007**, *457*, 111−122.
(19) Condò, I.; Malisan, F.; Guccini, I.; Serio, D.; Rufini, A.; Testi, R. Molecular control of the cytosolic aconitase/IRP1 switch by extramitochondrial frataxin. *Hum. Mol. Genet.* **2010**, *19*, 1221−1229.
(20) Rufini, A.; Fortuni, S.; Arcuri, G.; Condò, I.; Serio, D.; Incani, O.; Malisan, F.; Ventura, N.; Testi, R. Preventing the ubiquitin−proteasome-dependent degradation of frataxin, the protein defective in Friedreich's ataxia. *Hum. Mol. Genet.* **2011**, *20*, 1253−1261.
(21) Dominguez, C.; Boelens, R.; Bonvin, A. HADDOCK: a protein−protein docking approach based on biochemical or biophysical information. *J. Am. Chem. Soc.* **2003**, *125*, 1731−1737.
(22) Dijk, A.; Fushman, D.; Bonvin, A. Various strategies of using residual dipolar couplings in NMR driven protein docking: application to Lys48-linked di-ubiquitin and validation against ^{15}N-relaxation data. *Proteins* **2005**, *60*, 367−381.
(23) Dhe-Paganon, S.; Shigeta, R.; Chi, Y. I.; Ristow, M.; Shoelson, S. E. Crystal structure of human frataxin. *J. Biol. Chem.* **2000**, *275*, 30753−30756.
(24) Vijay-Kumar, S.; Bugg, C. E.; Cook, W. J. Structure of ubiquitin refined at 1.8 Å resolution. *J. Mol. Biol.* **1987**, *194*, 531−544.
(25) de Vries, S. J.; van Dijk, A. D. J.; Bonvin, A. M. WHISCY: What information does surface conservation yield? Application to data-driven docking. *Proteins* **2006**, *63*, 479−489.
(26) Neuvirth, H.; Raz, R.; Schreiber, G. ProMate: a structure based prediction program to identify the location of protein−protein binding sites. *J. Mol. Biol.* **2004**, *338*, 181−199.
(27) Swanson, K. A.; Kang, R. S.; Stamenova, S. D.; Hicke, L.; Radhakrishnan, I. Solution structure of Vps27 UIM-ubiquitin complex important for endosomal sorting and receptor downregulation. *EMBO J.* **2003**, *22*, 4597−4606.
(28) Lee, S.; Tsai, Y. C.; Mattera, R.; Smith, W. J.; Kostelansky, M. S.; Weissman, A. M.; Bonifacino, J. S.; Hurley, J. H. Structural basis for ubiquitin recognition and autoubiquitination by Rabex-5. *Nat. Struct. Mol. Biol.* **2006**, *13*, 264−271.
(29) Schmucker, S.; Martelli, A.; Colin, F.; Page, A.; Wattenhofer-Donzé, M.; Reutenauer, L.; Puccio, H. Mammalian frataxin: an essential function for cellular viability through an interaction with a preformed ISCU/NFS1/ISD11 iron−sulfur assembly complex. *PLoS One* **2011**, *6*, e16199.
(30) Leidgens, S.; De Smet, S.; Foury, F. Frataxin interacts with Isu1 through a conserved tryptophan in its β-sheet. *Hum. Mol. Genet.* **2010**, *19*, 276−286.
(31) Shan, Y.; Napoli, E.; Cortopassi, G. A. Mitochondrial frataxin interacts with ISD11 of the NFS1/ISCU complex and multiple mitochondrial chaperones. *Hum. Mol. Genet.* **2007**, *16*, 929−941.
(32) Tsai, C. L.; Bridwell-Rabb, J.; Barondeau, D. P. Friedreich's ataxia variants I154F and W155R diminish frataxin-based activation of the iron−sulfur cluster assembly complex. *Biochemistry* **2011**, *50*, 6478−6487.
(33) Developmental Therapeutics Program, National Cancer Institute. http://dtp.cancer.gov/.
(34) Charifson, P. S.; Walters, W. P. Filtering databases and chemical libraries. *J. Comput.-Aided Mol. Des.* **2002**, *16*, 311−323.
(35) Oprea, T. I.; Bologa, C.; Olah, M.; Alvarez, J.; Shoichet, B. Compound Selection for Virtual Screening. In *Virtual Screening in Drug Discovery*, Eds.; Taylor & Francis: Boca Raton, FL, 2005; pp 89−106.
(36) *FILTER*, version 2.0.1; OpenEye Scientific Software Inc.: Santa Fe, NM; http://www.eyesopen.com (accessed Sep 2009).
(37) *GLIDE*, version 5.7; Schrodinger, LLC: New York, 2011; http://www.schrodinger.com/.
(38) Morris, G. M.; Goodsell, D. S.; Halliday, R. S.; Huey, R.; Hart, W. E.; Belew, R. K.; Olson, A. J. Automated docking using a Lamarckian genetic algorithm and an empirical binding free energy function. *J. Comput. Chem.* **1998**, *19*, 1639−1662.
(39) Jacques, J.; Collet, A.; Wilen, S. H. *Enantiomers, Racemates, and Resolutions*; Wiley: New York, 1981.
(40) Nikolic, D.; Habibi-Goudarzi, S.; Corley, D. G.; Gafner, S.; Pezzuto, J. M.; Van Breemen, R. B. Evaluation of cyclooxygenase-2 inhibitors using pulsed ultrafiltration mass spectrometry. *Anal. Chem.* **2000**, *72*, 3853−3859.
(41) Liu, D.; Guo, J.; Luo, Y.; Broderick, D. J.; Schimerlik, M. I.; Pezzuto, J. M.; Breemen, R. B. Screening for ligands of human retinoid X receptor-alpha using ultrafiltration mass spectrometry. *Anal. Chem.* **2007**, *79*, 9398−9402.
(42) Berman, H. M.; Westbrook, J.; Feng, Z.; Gilliland, G.; Bhat, T. N.; Weissig, H.; Shindyalov, I. N.; Bourne, P. E. The Protein Data Bank. *Nucleic Acids Res.* **2000**, *28*, 235−242.
(43) Sander, C.; Schneider, R. Database of homology-derived protein structures and the structural meaning of sequence alignment. *Proteins* **1991**, *9*, 56−68.
(44) Linge, J. P.; Williams, M. A.; Spronk, C. A.; Bonvin, A. M.; Nilges, M. Refinement of protein structures in explicit solvent. *Proteins* **2003**, *50*, 496−506.

(45) Jorgensen, W. L.; Tirado-Rives, J. The OPLS potential function for proteins. Energy minimization for crystals of cyclic peptides and crambin. *J. Am. Chem. Soc.* **1998**, *110*, 1657−1666.
(46) McDonald, I. K.; Thornton, J. M. Satisfying hydrogen bonding potential in proteins. *J. Mol. Biol.* **1994**, *238*, 777−793.
(47) Irwin, J. J.; Shoichet, B. K. ZINC—a free database of commercially available compounds for virtual screening. *J. Chem. Inf. Model.* **2005**, *45*, 177−182.
(48) Charifson, P. S.; Corkery, J. J.; Murcko, M. A.; Walters, W. P. Consensus scoring: a method for obtaining improved hit rates from docking databases of three-dimensional structures into proteins. *J. Med. Chem.* **1999**, *42*, 5100−5109.
(49) Oda, A.; Tsuchida, K.; Takakura, T.; Yamaotsu, N.; Hirono, S. Comparison of consensus scoring strategies for evaluating computational models of protein−ligand complexes. *J. Chem. Inf. Model.* **2006**, *46*, 380−391.
(50) *QikProp*, version 3.4; Schrödinger LLC: New York, 2011.
(51) Ihlenfeldt, W. D.; Voigt, J. H.; Bienfait, B.; Oellien, F.; Nicklaus, M. C. Enhanced CACTVS browser of the open NCI database. *J. Chem. Inf. Comput. Sci.* **2002**, *42*, 46−57.
(52) Willett, P. Similarity-based approaches to virtual screening. *Biochem. Soc. Trans.* **2003**, *31*, 603−606.
(53) Martin, Y. C.; Kofron, J. L.; Traphagen, L. M. Do structurally similar molecules have similar biological activity? *J. Med. Chem.* **2002**, *45*, 4350−4358.